Two-dimensional solitons in quasi-phase-matched quadratic crystals

N.-C. Panoiu,[1,*] D. Mihalache,[2,3] D. Mazilu,[2,3] F. Lederer,[3] and R. M. Osgood, Jr.[1,†]

[1]*Department of Applied Physics and Applied Mathematics, Columbia University, New York, New York 10027, USA*
[2]*Department of Theoretical Physics, Institute of Atomic Physics, P.O. Box MG-6, Bucharest, Romania*
[3]*Institute of Solid State Theory and Theoretical Optics, Friedrich Schiller University Jena, Max-Wien-Platz 1,
D-07743 Jena, Germany*

We study the existence and dynamics of two-dimensional spatial solitons in crystals that exhibit a periodic modulation of both the refractive index and the second-order susceptibility for achieving quasi-phase-matching. Far from resonances between the domain length of the periodic crystal and the diffraction length of the beams, it is demonstrated that the properties of the solitons in this quasi-phase-matched geometry are strongly influenced by the induced third-order nonlinearities. The stability properties of the two-dimensional solitons are analyzed as a function of the total power, the effective wave-vector mismatch between the first and second harmonics, and the relative strength between the induced third-order nonlinearity and the effective second-order nonlinearity. Finally, the formation of two-dimensional solitons from a Gaussian beam excitation is investigated numerically.

I. INTRODUCTION

It has been known since the early days of nonlinear optics that the cascading of two second-order processes, such as up- and down-conversion in a three wave mixing process, generally leads to nonlinear phase shifts of all waves involved [1–3]. However, only recently has this phase modulation been analyzed systematically [4]. In Ref. [4], it was found that the process depends primarily on the ratio of wave-vector mismatch and effective second-order susceptibility. This phenomenon also displays some unusual physical properties [4]; for instance, its effect may exceed appreciably the phase modulation obtained with intrinsic cubic nonlinearities. If the wave-vector mismatch is large, this phase shift resembles that achieved with an effective third-order nonlinearity and typical nonlinear effects, usually induced by cubic nonlinearities, such as all-optical switching, optical limiting, or soliton formation have been demonstrated [5–10].

During the past few years, intense research activity has focused on both the experimental and theoretical investigations of phenomena related to these cascaded second-order processes and their potential use for all-optical applications. Thus, a large phase modulation was measured in several experimental setups, such as bulk KTP [5] and Ti-indiffused LiNbO$_3$ [11] or KTP [7] channel waveguides. Furthermore, the potential use of this effect to all-optical switching in a Mach-Zender interferometer [9] or phase-controlled transistor action [12] has also been experimentally demonstrated. With regard to theory, many schemes to achieve phase and amplitude modulation through cascading second-order interaction have been proposed [4,8,13–15] and their use to optical transistors [12,16–20], loop mirrors [21], or nonlinear

directional couplers [15] has been suggested.

As indicated above, the wave-vector mismatch is a key parameter that controls the character of quadratic interaction. There are several techniques for controlling wave-vector matching of the waves propagating in a quadratic medium so as to achieve phase-matching. For instance, birefringence-based phase-matching techniques (PMT) use the anisotropic nature of the dispersion relation $\mathbf{k}(\omega)$ to cancel the vector mismatch between the fundamental wave (FW) and the second harmonic (SH), which propagate at ω and 2ω, respectively [22]. Another traditional PMT is based on temperature tuning of waveguide dispersion, i.e., modal PMT [23]. Finally, quasi-phase-matching (QPM) is a powerful technique, consisting of compensating the wave-vector mismatch through artificial periodic variation of the quadratic nonlinear coefficient $\chi^{(2)}$. The QPM technique offers several advantages: it uses the highest possible $\chi^{(2)}$ coefficients; it eliminates the spatial walk-off effects; it can use nonbirefringent materials; phase matching can be achieved at room temperature; and it allows higher flexibility in choosing the configuration of interacting waves, e.g., one can phase-match counterpropagating waves.

Although the QPM technique was proposed in the seminal paper of Armstrong *et al.* almost four decades ago [1], recent technological progresses allowed the routine fabrication of high quality QPM gratings. There are two major classes of QPM structure. Those in the first class consist in alternating domains whose sign of the $\chi^{(2)}$ coefficient changes every semiperiod. They are obtained by standard poling techniques of LiNbO$_3$ or KTP crystals [24–26] or waveguides [27,28] or, in the case of QPM gratings with slab waveguide geometry, by a poling procedure followed by crystal ion slicing [29]. We will term this type of structures symmetric gratings (SG). QPM structures of the second class will be termed asymmetric gratings (AG) and can involve a periodic modulation either of the $\chi^{(2)}$ coefficient alone, by use of alternating quantum wells [30], or of both refractive index and $\chi^{(2)}$ coefficient, by stacking together thin slabs of different semi-

---

*On leave from Department of Theoretical Physics, Institute of Atomic Physics, P.O. Box MG-6, Bucharest, Romania.

†Formerly at Brookhaven National Laboratories, Upton, New York, 11973.

conductor crystals [31,32]. Finally, since they exhibit huge nonlinearities, polymer materials can also be used to fabricate QPM gratings [33].

Over the last few years, soliton formation in quadratic media has been the ground of intense research activity, both experimental and theoretical. Thus, in addition to the first experimental verification of soliton existence in a bulk KTP crystal [34] and LiNbO$_3$ slab waveguides [35], the existence and stability of soliton propagation in quadratic media have been demonstrated for various geometries: spatial solitons in slab waveguides [36] or bulk crystals [37–39] and walking solitons in slab waveguides [40] or bulk crystals [41]. Several theoretical studies have been reported on one-dimensional spatial soliton propagation in QPM waveguides [42,43]. These studies have shown that the periodic modulation of the quadratic nonlinearity induces an artificial cubic nonlinearity that can compete with the former one. A discussion of this phenomenon as well as an analysis of the validity of the theory describing this effect can be found in Ref. [44]. Furthermore, it has been demonstrated that by modulating the grating the induced third-order nonlinearity can be further increased [45]; a switching scheme based on this effect has been proposed in Ref. [46]. The first experimental verification of two-dimensional soliton formation in QPM gratings was reported in Ref. [47]. For a comprehensive review on quadratic solitons, see Ref. [48].

In this paper we present, to our knowledge for the first time, a theoretical analysis of 2D soliton formation and their stability upon propagation in QPM gratings, by taking into account the higher-order nonlinearities induced by the periodicity of the grating [42]. We consider both SG, for which the average $\chi^{(2)}$ coefficient vanishes, as well AG, for which both the average $\chi^{(2)}$ coefficient and the modulation of the refractive indices are nonzero. The paper is organized as follows. In the following section we introduce the mathematical model that describes the nonlinear interaction between two cw beams propagating in a QPM grating. Then, in Sec. III, we find, numerically, the QPM solitons that are stable upon propagation in the QPM grating and the influence of the induced third-order nonlinearities on their properties. Furthermore, a detailed stability analysis of the QPM solitons is presented in Sec. IV. In Sec. V, we investigate the excitation of these QPM solitons, using Gaussian beams. Two situations are taken into account: launching of both harmonics [seeded second harmonic generation (SHG)] or of only the FW (unseeded SHG). Finally, we conclude with a summary and discussion of our results.

II. MATHEMATICAL MODEL

We consider the propagation in a lossless QPM grating, under type-I SHG conditions, of a cw beam at frequency ω and its SH at frequency 2ω. The QPM grating consists of a periodic structure, for which both the linear part of the susceptibility (refractive index) and the quadratic susceptibility are periodic functions of the longitudinal distance, as it is illustrated in Fig. 1. In this geometry, both the FW and the SH are polarized along the same direction, which is also a principal crystal axis; therefore, no walk-off effects are
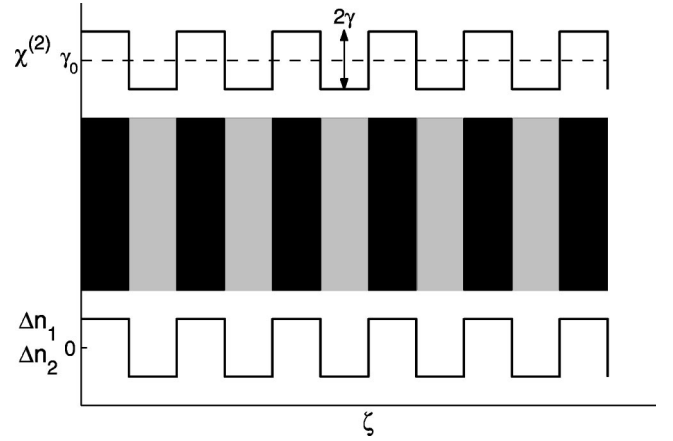

FIG. 1. Schematic presentation of a QPM grating: γ_0 is the average value of the quadratic nonlinearity, γ is its modulation amplitude, and Δn_1 and Δn_2 are the deviations from the mean value of the refractive indices at the FW and SH, respectively.

present. Since we want to describe both SG and AG, we allow for the averaged (normalized) quadratic susceptibility coefficient γ_0 to be nonzero, a situation that describes QPM gratings fabricated from semiconductor materials. We consider that the two co-propagating fields are plane waves propagating along the z direction,

$$\mathbf{E}_i(\mathbf{r},t) = \frac{1}{2}\hat{\mathbf{e}}E_i(x,y,z)\exp[i(\omega_i t - k_i z)] + \text{c.c.}, \qquad (1)$$

where $\hat{\mathbf{e}}$ is a unit vector along the polarization direction, x and y are the transverse coordinates, z is the longitudinal distance, $\omega_1 = \omega$, $\omega_2 = 2\omega$, and E_i and $k_i = k(\omega_i)$ are the electric fields and wave vectors at the two harmonics, respectively. Then, within the slowly varying envelope approximation, the two co-propagating fields obey the following system of equations [49]:

$$2ik_1\frac{\partial E_1}{\partial z} + \nabla_\perp^2 E_1 + \frac{2\omega_1^2 \bar{n}_1}{c^2}\phi\Delta n_1(z)E_1$$

$$+ \frac{2\omega_1^2}{c^2}\chi^{(2)}(z)E_1^* E_2 \exp(-i\Delta kz) = 0, \qquad (2a)$$

$$2ik_2\frac{\partial E_2}{\partial z} + \nabla_\perp^2 E_2 + \frac{2\omega_2^2 \bar{n}_2}{c^2}\Delta n_2(z)E_2$$

$$+ \frac{\omega_2^2}{c^2}\chi^{(2)}(z)E_1^2 \exp(i\Delta kz) = 0, \qquad (2b)$$

where $\nabla_\perp^2$ is the transverse Laplacian, $\Delta k = 2k_1 - k_2$ is the wave-vector mismatch, $\chi^{(2)}(z)$ is the quadratic nonlinear coefficient and is z dependent, $\bar{n}_1, \bar{n}_2$ and $\Delta n_1(z), \Delta n_2(z)$ are, respectively, the averages and the modulations of the two refractive indices at the FW and the SH.

In order to normalize this system, we introduce a new set of normalized variables and functions: $\zeta = z/z_0$, $\eta = x/w_0$,

$\xi = y/w_0$, $u = A_1 E_1$, and $v = A_2 E_2$. Here, $z_0 = k_1 w_0^2$ is the diffraction length, w_0 is the characteristic beam width, and $A_i = \sqrt{\epsilon_0 c \bar{n}_i / 2 S_0}$ are normalization constants, with c being the speed of light, ϵ_0 the vacuum permittivity, and $S_0 = 1$ GW/cm^2 a normalization intensity. Upon normalization, the system of equations (2) becomes

$$i\frac{\partial u}{\partial \zeta} + \frac{1}{2}\nabla_\perp^2 u + \alpha_u(\zeta)u + \Gamma(\zeta)u^* v \exp(-i\beta\zeta) = 0, \tag{3a}$$

$$i\frac{\partial v}{\partial \zeta} + \frac{1}{4}\nabla_\perp^2 v + 2\alpha_v(\zeta)v + \Gamma(\zeta)u^2 \exp(i\beta\zeta) = 0, \tag{3b}$$

where $\beta = z_0 \Delta k$ is the normalized wave vector mismatch, $\alpha_{u,v}(\zeta) = \omega z_0 \Delta n_{1,2}(\zeta)/c$ are the normalized modulations of the refractive indices [for a SG, $\alpha_{u,v}(\zeta) \equiv 0$ and $\gamma_0 = 0$], and $\Gamma(\zeta) = (\omega z_0 \chi^{(2)}/c)\sqrt{2S_0/\epsilon_0 c \bar{n}_1^2 \bar{n}_2}$ is the normalized parametric coupling strength.

For the sake of simplicity, in what follows we assume that the functions $\alpha_{u,v}(\zeta)$ and $\Gamma(\zeta)$ that characterize the QPM grating are single-periodic functions. For reasons that will be discussed later, more complex choices have been proposed in other studies, e.g., multi- [45,50] or quasiperiodic [43] functions. With this choice, there are three physical lengths that characterize the system, and the interplay among these characteristic lengths determines the dynamics of the interacting beams. These three lengths are the diffraction length z_0, the coherence length $L_c = \pi/|\Delta k|$, and the domain length Λ. In normalized units, $z_0 = 1$ and $L_c = \pi/|\beta|$. We consider here a typical QPM grating for which the domain length is much smaller than the diffraction length, that is, $\Lambda \ll 1$. Then, the grating wave vector defined by $|\kappa| = \pi/\Lambda$ satisfies the relation $|\kappa| \gg 1$, implying that $1/|\kappa|$ is a normalized characteristic length that is much smaller than 1.

In order to analyze the beam propagation in the QPM grating, we use an asymptotic expansion technique introduced in Ref. [42]. To this end, we expand in Fourier series the grating functions $\Gamma(\zeta)$ and $\alpha_{u,v}(\zeta)$, and the fields $u(\eta,\xi;\zeta)$ and $v(\eta,\xi;\zeta)$:

$$\Gamma(\zeta) = \gamma_0 + \gamma\sum_n g_n e^{in\kappa\zeta}, \tag{4a}$$

$$\alpha_{u,v}(\zeta) = a_{u,v}\sum_n g_n e^{in\kappa\zeta}, \tag{4b}$$

$$u(\eta,\xi;\zeta) = \sum_n u_n(\eta,\xi;\zeta)e^{in\kappa\zeta}, \tag{4c}$$

$$v(\eta,\xi;\zeta) = \sum_n v_n(\eta,\xi;\zeta)e^{i(n\kappa+\bar{\beta})\zeta}, \tag{}$$

where γ_0 and γ are, respectively, the average and the modulation amplitudes of the parametric coupling strength, $a_{u,v}$ are the amplitudes of the modulation of the refractive index at the frequencies of the two harmonics, $u_n(\eta,\xi;\zeta)$ and

$v_n(\eta,\xi;\zeta)$ are slowly varying functions with respect to the variables, as compared to the exponential, and $\bar{\beta} = \beta - \kappa$ is the effective phase mismatch parameter. We assume that the phase mismatch introduced by the QPM grating can be very well controlled, so that $\bar{\beta}$ is very small (although both β and $|\kappa|$ must be large). For the geometry in Fig. 1, the Fourier coefficients g_n are given by the expression

$$g_n = \begin{cases} \dfrac{2\,\mathrm{sgn}(\kappa)}{i\pi n}, & n \text{ odd} \\ 0, & n \text{ even.} \end{cases} \tag{5}$$

Here, the $\mathrm{sgn}(\kappa)$ factor ensures that both positive and negative values of κ correspond to the same grating. Consequently, since $\mathrm{sgn}(\beta) = \mathrm{sgn}(\kappa)$, we can treat both cases $\beta \lessgtr 0$ at the same time.

Now, we assume that the higher harmonics in expansions (4c) are of the order $O(1/|\kappa|)$ or smaller, whereas u_0 and v_0 are of the order $O(1)$. Then, inserting expressions (4a)–(4c) in system (3) and collecting all terms of the order $O(1)$, we obtain the relationships between the higher-order Fourier coefficients and the zero-order ones (or, as called in this paper, the average fields), u_0 and v_0:

$$u_{n\neq 0} = \frac{1}{n\kappa}[a_u g_n u_0 + (\gamma_0 \delta_{n,-1} + \gamma g_{n+1})u_0^* v_0], \tag{6a}$$

$$v_{n\neq 0} = \frac{1}{n\kappa}[2a_v g_n v_0 + (\gamma_0 \delta_{n,1} + \gamma g_{n-1})u_0^2]. \tag{6b}$$

Then, by inserting these expressions in system (3) and neglecting higher-order terms in the corresponding system that describes the evolution of the zero-order fields, we end up with the following system of equations that describes the evolution of the zero-order fields:

$$i\frac{\partial u_0}{\partial \zeta} + \frac{1}{2}\nabla_\perp^2 u_0 + \rho u_0^* v_0 + \delta(|u_0|^2 - |v_0|^2)u_0 = 0, \tag{7a}$$

$$i\frac{\partial v_0}{\partial \zeta} + \frac{1}{4}\nabla_\perp^2 v_0 - \bar{\beta}v_0 + \rho^* u_0^2 - 2\delta|u_0|^2 v_0 = 0. \tag{7b}$$

Here, ρ is the effective second-order nonlinearity and is given by

$$\rho = \frac{2i\,\mathrm{sgn}(\kappa)}{\pi}\left[\frac{2\gamma_0}{\kappa}(a_u - a_v) - \gamma\right], \tag{8}$$

and δ characterizes the magnitude of the induced third-order nonlinearity, and can be written as

$$\delta = \frac{1}{\kappa}\left[\gamma_0^2 + \gamma^2\left(1 - \frac{8}{\pi^2}\right)\right]. \tag{9}$$

Equations (7), with the Laplacian replaced by transverse second-order derivative, were first derived in Ref. [42], to describe the 1D case. Equation (8) shows that the effective second-order nonlinearity in a SG ($\gamma_0 = 0$) is decreased by a

factor of $2/\pi$, as compared to the case of bulk crystal, a well-known result. However, the most important consequence of the averaging procedure is the appearance of an induced effective third-order nonlinearity, similar to a Kerr effect. There is, though, an important difference: the self-phase and cross-phase modulation terms have opposite signs. This means that by tuning the parameters of the QPM grating one can obtain either focusing or defocusing third-order nonlinearities; this asymmetric structure of the induced higher-order nonlinearities has been recently verified experimentally [51].

III. QPM SOLITONS

In this section we introduce the soliton solutions of system (7) and discuss their physical properties. To begin with, we rescale the fields u_0 and v_0 by the effective second-order nonlinearity ρ, $u_0 = \tilde{u}_0/|\rho|$, $v_0 = \tilde{v}_0/\rho$. Then, system (7) becomes

$$i\frac{\partial \tilde{u}_0}{\partial \zeta} + \frac{1}{2}\nabla_\perp^2 \tilde{u}_0 + \tilde{u}_0^* \tilde{v}_0 + \sigma(|\tilde{u}_0|^2 - |\tilde{v}_0|^2)\tilde{u}_0 = 0, \quad (10\text{a})$$

$$i\frac{\partial \tilde{v}_0}{\partial \zeta} + \frac{1}{4}\nabla_\perp^2 \tilde{v}_0 - \bar{\beta}\tilde{v}_0 + \tilde{u}_0^2 - 2\sigma|\tilde{u}_0|^2 \tilde{v}_0 = 0, \quad (10\text{b})$$

where $\sigma = \delta/|\rho|^2$ gives the relative strength between the induced cubic nonlinearity and the effective quadratic nonlinearity. For typical SG, the parameter $\sigma \lesssim 0.05$, but, as we will show later, even such relatively small values can have a dramatic influence on the soliton formation process. Moreover, for AG or certain specially engineered gratings [45,50], the parameter σ can become close to 1. Furthermore, it is important to mention that the parameter σ is determined only by the parameters $x = \gamma_0/\gamma$, $p = (a_u - a_v)/\kappa$, and the grating wave vector κ:

$$\sigma = \frac{1}{4\kappa} \frac{\pi^2(x^2+1)-8}{(2px-1)^2}. \quad (11)$$

In what follows, we look for solitary solutions (solitons) of system (10), which are localized stationary solutions of the form

$$\tilde{u}_0(\eta,\xi;\zeta) = \bar{u}_0(r)e^{i\lambda\zeta}, \quad \tilde{v}_0(\eta,\xi;\zeta) = \bar{v}_0(r)e^{2i\lambda\zeta}, \quad (12)$$

where the parameter λ is the soliton wave vector and $r = \sqrt{\eta^2 + \xi^2}$. Since we assumed that the functions $u_0(\eta,\xi;\zeta)$ and $v_0(\eta,\xi;\zeta)$ vary slowly as compared to $e^{i\kappa\zeta}$, the soliton parameter λ must be much smaller than κ. Here, we consider only lowest-order solutions (with no nodes) with radial symmetry. Moreover, we consider only the case in which both the functions are real and neither of the two solutions, $\bar{u}_0(r)$ and $\bar{v}_0(r)$, is identically equal to 0. Although from a rigorous purely mathematical point of view these solutions

are not soliton solutions of system (10) [52], we will follow the terminology in the physics literature and call them solitons.

By inserting Eqs. (12) in Eqs. (10), one can readily verify that the soliton solutions are given by the following system of equations:

$$\frac{1}{2}\nabla_\perp^2 \bar{u}_0 - \lambda\bar{u}_0 + \bar{u}_0\bar{v}_0 + \sigma(\bar{u}_0^2 - \bar{v}_0^2)\bar{u}_0 = 0, \quad (13\text{a})$$

$$\frac{1}{4}\nabla_\perp^2 \bar{v}_0 - (2\lambda + \bar{\beta})\bar{v}_0 + \bar{u}_0^2 - 2\sigma\bar{u}_0^2\bar{v}_0 = 0. \quad (13\text{b})$$

Furthermore, from the expansions in Eq. (4c), and by using relations (6), one can see that, at the first-order in the smallness of parameter $\epsilon = 1/|\kappa|$, the soliton solutions of full system (3) and those of averaged system (10) are related by the following relations:

$$u(\eta,\xi;0) = \frac{\bar{u}_0(r)}{|\rho|} - \frac{1}{|\kappa|}\left[\frac{i\pi a_u}{2} + \left(\frac{2i\gamma}{\pi} + \gamma_0\,\text{sgn}(\kappa)\right)\frac{\bar{v}_0(r)}{\rho}\right]$$

$$\times \frac{\bar{u}_0(r)}{|\rho|} + O\left(\frac{1}{|\kappa|^2}\right), \quad (14\text{a})$$

$$v(\eta,\xi;0) = \frac{\bar{v}_0(r)}{\rho} - \frac{1}{|\kappa|}\left[i\pi a_v \frac{\bar{v}_0(r)}{\rho}\right.$$

$$\left. + \left(\frac{2i\gamma}{\pi} - \gamma_0\,\text{sgn}(\kappa)\right)\frac{\bar{u}_0^2(r)}{|\rho|^2}\right] + O\left(\frac{1}{|\kappa|^2}\right).$$

$$(14\text{b})$$

The existence and dynamics of QPM soliton solutions of full system (3) are studied by finding first the soliton solutions of system (10), whose coefficients do not depend on the longitudinal distance ζ, and then by using relations (14) to obtain the soliton solutions of full system (3), at $\zeta = 0$. We call the solitons of system (10) zero-order solitons, whereas those obtained from the zero-order ones through transformation (14) are called first-order solitons. Thus, the zero-order solitons are obtained by keeping the terms of order $O(1)$ in Eqs. (14), whereas the first-order solitons are obtained from Eqs. (14) by keeping all the terms up to the order $O(1/|\kappa|)$. Then, in order to analyze the stability properties of these solitons, they are propagated in the grating by integrating numerically full system (3).

For numerical integration we used a standard Crank-Nicolson method, with transparent boundary conditions imposed at frontiers [53]. Typically, at each longitudinal step, four Picard iterations and ten Gauss-Seidel iterations were needed. The stationary solutions of system (10), that is, the solutions of system (13), are determined numerically by using a standard band-matrix method with Newton-type iterations [54]. Since we look for solutions with radial symmetry, system (13) can be formulated such that only one transverse coordinate r enters. This reduction considerably simplifies the computation.

FIG. 4. Amplitudes (upper row) and the corresponding intensities (lower row) evolution, in a SG, of the zero-order (left column) and first-order (right column). Soliton propagation is described by full system (3). The soliton parameters are as in Fig. 3.
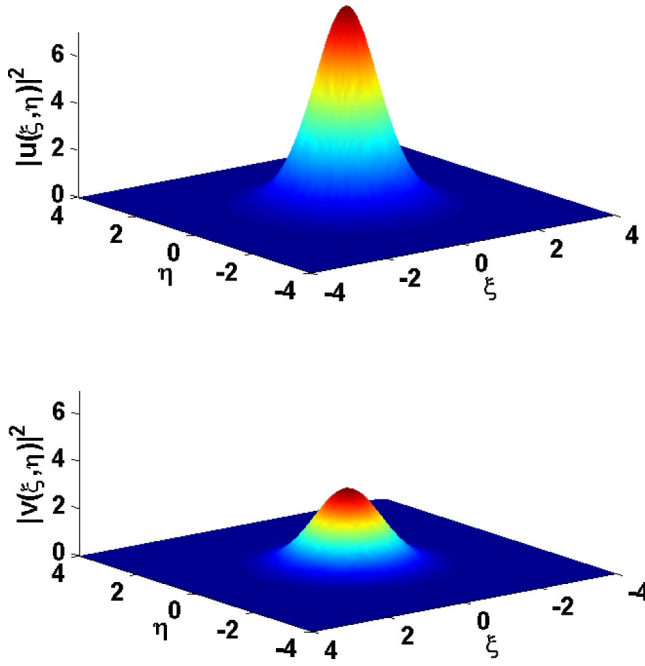

FIG. 2. (Color online) First-order QPM solitons of full system (3), obtained from the solitons of averaged system (10) by applying transformations (14). The soliton parameters are $\lambda = 0.5$, $\sigma = 0.05$, and $\bar{\beta} = 0$ (phase-matched solitons).

We applied this method and determined soliton solutions of system (3). A typical example is presented in Figs. 2 and 3. Thus, Fig. 2 presents a soliton solution obtained by applying transformation (14) to a soliton solution of averaged system (10) and keeping all the terms up to the order $O(1/|\kappa|)$, that is, the first-order solitons. The zero-order solitons are
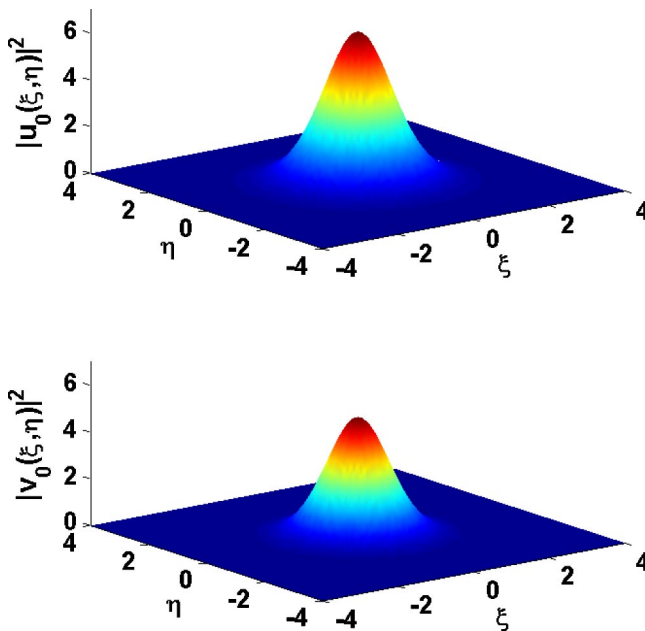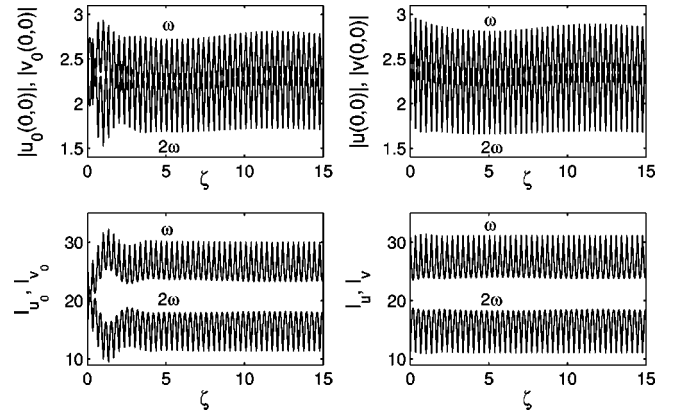

FIG. 3. (Color online) Soliton solutions for averaged system (13). The soliton parameters are $\lambda = 0.5$, $\sigma = 0.05$, and $\bar{\beta} = 0$ (the same as in Fig. 2).

shown in Fig. 3. Note that in the case of approximate solitons, that is, zero-order solutions, the difference in the soliton amplitudes at the two harmonics is smaller as compared to the first-order soliton.

Before analyzing in more detail how these solitons propagate in a QPM grating, note that one set of parameters that defines a soliton solution of system (10) corresponds to an entire family of QPM gratings, characterized by this set of parameters. More exactly, there is an infinite set of choices of the grating parameters x, p, and κ that correspond to the same value of the induced cubic nonlinearity strength σ. Therefore, the solitons we analyze here, characterized by a certain parameter σ, can be excited in a multitude of QPM gratings of different types, e.g., in both SG and AG.

In order to study the validity of our perturbative approach, we numerically integrated full system (3), using as initial conditions both the zero-order soliton and the soliton obtained from the zero-order one by using expressions (14), that is, the first-order soliton. We used two types of gratings: first, a SG characterized by the parameters $a_u = a_v = 0$, $\gamma_0 = 0$, $\gamma = 1$, and $\kappa = 9.35$; the second, an AG grating, with the parameters $a_u = 1$, $a_v = 1.928$, $\gamma_0 = 1$, $\gamma = 0.4$, and $\kappa = 308.42$. Both these sets of parameters correspond to the same $\sigma = 0.05$. We monitored both the amplitudes of the solitons as well as their intensities. The intensities at the two harmonics, as well as the total intensity, are defined by the following expressions:

$$I_{\tilde{u}_0} = \int |\tilde{u}_0(\eta, \xi; \zeta)|^2 d\eta d\xi, \tag{15a}$$

$$I_{\tilde{v}_0} = \int |\tilde{v}_0(\eta, \xi; \zeta)|^2 d\eta d\xi, \tag{15b}$$

$$\tilde{I}_0 = I_{\tilde{u}_0} + I_{\tilde{v}_0}. \tag{15c}$$

An important property of the intensity $\tilde{I}_0$, which can be easily derived from system (10), is that it is independent of the longitudinal distance ζ, that is, it is a conserved quantity.

We present in Fig. 4 the soliton propagation in a SG characterized by the parameters given above. Note that in this
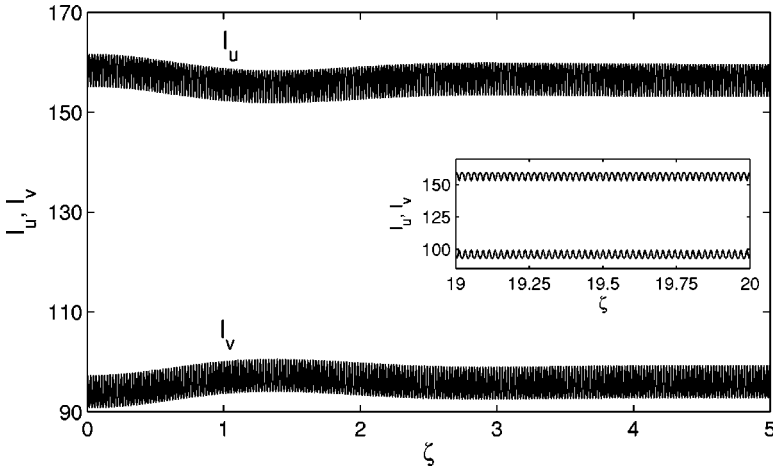
FIG. 5. Evolution of first-order soliton intensities upon propagation in an AG. In the inset, soliton propagation over a diffraction length, after the steady state is reached. The soliton parameters are as in Fig. 3.

figure the intensities I_{u_0}, I_{v_0} and I_u, I_v represent the beam intensities described by full system (3) and correspond, respectively, to the zero-order and second-order solitons defined earlier. To be more specific, to calculate I_{u_0} and I_{v_0} we used the zero-order soliton as initial condition for full system (3) and integrated it numerically. Then, the intensities I_{u_0} and I_{v_0} were calculated by integrating the propagating fields; the intensities I_u and I_v were calculated in a similar way except that as initial conditions we used the first-order solitons. Figure 4 illustrates that, even the zero-order soliton solution is a very good approximation for the QPM soliton that is formed upon propagation in the grating. Thus, in the case of zero-order approximation, a soliton is formed after just a few diffraction lengths, whereas in the case in which the first-order soliton is launched into the QPM grating the transient regime can hardly be observed. We observed that in both cases the amount of energy radiated during the transient regime is negligible. This means that even in the case of zero-order soliton, during the initial stage of the propagation, the energy is not radiated but, in fact, is redistributed between the two harmonics.

The fast oscillations of the beam intensities, shown in Fig. 4, can be understood by noting the relationship between the intensities of the fields $u(\eta, \xi; \zeta)$ and $v(\eta, \xi; \zeta)$, and the intensities corresponding to the averaged fields $I_{\tilde{u}_0}$ and $I_{\tilde{v}_0}$. Thus, by using expansions (4c) and definitions (15a) and (15b), one obtains the following relations:

$$I_u = \frac{I_{\tilde{u}_0}}{|\rho|^2} + \frac{2iK}{\kappa|\rho|^2\rho}\left[\gamma_0 \sin(\kappa\zeta) - \frac{4\,\mathrm{sgn}(\kappa)}{\pi}\sum_{n\geq1}\frac{\cos(2n\kappa\zeta)}{4n^2-1}\right]$$
$$+ O\left(\frac{1}{|\kappa|^2}\right), \tag{16a}$$

$$I_v = \frac{I_{\tilde{v}_0}}{|\rho|^2} - \frac{2iK}{\kappa|\rho|^2\rho}\left[\gamma_0 \sin(\kappa\zeta) - \frac{4\,\mathrm{sgn}(\kappa)}{\pi}\sum_{n\geq1}\frac{\cos(2n\kappa\zeta)}{4n^2-1}\right]$$
$$+ O\left(\frac{1}{|\kappa|^2}\right), \tag{16b}$$

where $K = \int \tilde{u}_0^2 \tilde{v}_0 \, d\eta \, d\xi$ is a constant. Similar relation have been derived in Ref. [42], for the particular case of 1D SG. These equations show that, over certain constant values of the intensities of the beams, $I_{\tilde{u}_0,\tilde{v}_0}/|\rho|^2$, there are superimposed fast modulations with the spatial frequency equal to 2κ. Their origin is the existence of higher nonzero terms in the Fourier expansion (4c). Note that in the case of AG ($\gamma_0 \neq 0$) the spatial frequency of the modulation of the intensities is equal to κ. Also, notice that the beam intensities at the zero- and first-order are conserved, that is, $I \equiv I_u + I_v = \tilde{I}_0/|\rho|^2$.

The same behavior is observed in Fig. 5, which shows the evolution of the first-order soliton upon propagation in an AG characterized by the parameters given above. In contrast to the previous case, the transient distance over which the input solitons reach a steady-state propagation is slightly larger. Also, notice the much larger spatial oscillation frequency that can be observed in this case. Obviously, this is due to the fact that in this case the grating periodicity is much smaller.

To gain a better understanding of the differences displayed upon propagation by the zero- and first-order approximations of the QPM solitons, we also determined the dependence of the total intensity and the Hamiltonian, on the longitudinal distance ζ; the results are shown in Fig. 6. The Hamiltonians H and H_0 are given by the following expressions:

$$H = \frac{1}{2}\int\left\{|\nabla_\perp\psi|^2 + \frac{1}{4}|\nabla_\perp\phi|^2 - 2\alpha_\psi(\zeta)|\psi|^2\right.$$
$$\left. - [2\alpha_\phi(\zeta) - \beta]|\phi|^2 - \Gamma(\zeta)(\psi^{*2}\phi + \phi^*\psi^2)\right\}d\eta\,d\xi, \tag{17a}$$

$$H_0 = \frac{1}{2}\int\left\{|\nabla_\perp\tilde{u}_0|^2 + \frac{1}{4}|\nabla_\perp\tilde{v}_0|^2 + \bar{\beta}|\tilde{v}_0|^2 - (\tilde{u}_0^{*2}\tilde{v}_0 + \tilde{v}_0^*\tilde{u}_0^2)\right.$$
$$\left. - 2\sigma\left(\frac{|\tilde{u}_0|^2}{2} - |\tilde{v}_0|^2\right)|\tilde{u}_0|^2\right\}d\eta\,d\xi, \tag{17b}$$
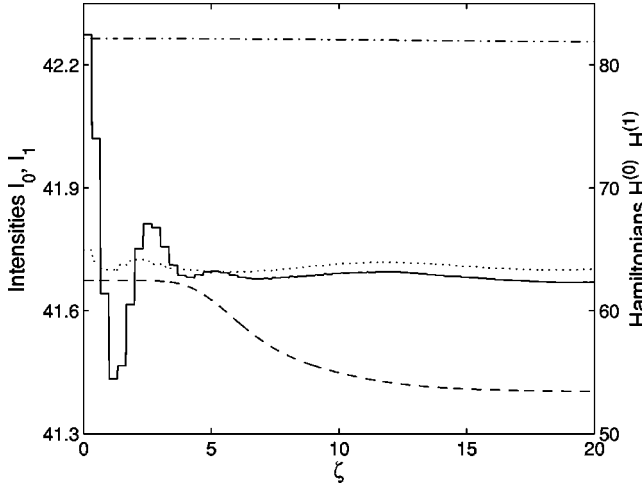
FIG. 6. Intensities (left axis) and Hamiltonians (right axis) vs the longitudinal distance ζ. Hamiltonian $H^{(0)}$ (—) and intensity I_0 (- - -) correspond to the zero-order soliton, whereas Hamiltonian $H^{(1)}$ ($\cdots$) and intensity I_1 ($-\cdot-$) correspond to the first-order soliton.

where $\psi = u$ and $\phi = v e^{i\beta\zeta}$. They correspond, respectively, to systems (3) and (10). In fact, systems (3) and (10) represent the Hamilton equations associated to the Hamiltonians (17); for example, Eqs. (10) are equivalent to the following canonical equations:

$$i\frac{\partial \tilde{u}_0}{\partial \zeta} = \frac{\delta H_0}{\delta \tilde{u}_0^*}, \tag{18a}$$

$$i\frac{\partial \tilde{v}_0}{\partial \zeta} = 2\frac{\delta H_0}{\delta \tilde{v}_0^*}, \tag{18b}$$

with a similar set of equations for H, ψ, and ϕ. Here, the symbol δ indicates a functional derivative. There is an important distinction between the two cases: while H_0 is a constant of motion, H depends on the longitudinal distance ζ. The fact that H is not conserved upon propagation is clearly seen in Fig. 6. Notice that both $H^{(0)}$ and $H^{(1)}$ shown in this figure have been computed by using the Hamiltonian H associated to full system (3). Thus, $H^{(0)}$ was calculated by using the zero-order soliton as initial condition, whereas $H^{(1)}$ was calculated by using the first-order soliton as initial condition. Furthermore, Fig. 6 shows that in the case of first-order approximation only a small amount of radiation is emitted. In contrast, in the case of zero-order approximation, part of the soliton energy is radiated before the soliton is reshaped to its steady-state form. The plateau at the beginning of the propagation signifies the fact that the radiation propagates over several diffraction lengths before it reaches the boundaries situated at $\eta_b, \xi_b = \pm 10$, and leaves the computational domain.

As has been discussed in Sec. II, an important consequence of the averaging process is the fact that the beams interact in the QPM grating as if they were under the influence of Kerr-type nonlinearities. In order to characterize quantitatively this effect, we found the QPM solitons that
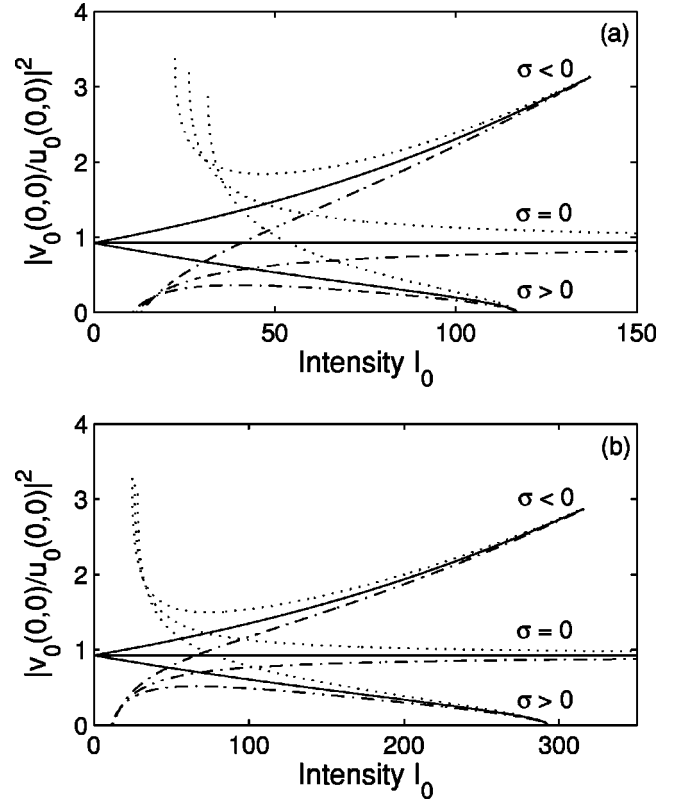

FIG. 7. Peak intensities' ratio of the soliton solutions of system (10), calculated for $\sigma = -0.05$, $\sigma = 0$, and $\sigma = 0.05$ (a) and $\sigma = -0.02$, $\sigma = 0$, and $\sigma = 0.02$ (b). The effective wave-vector mismatch is $\bar{\beta} = -2$ ($\cdots$), $\bar{\beta} = 0$ (—), and $\bar{\beta} = 2$ ($-\cdot-$).

correspond to system (10), for various values of the soliton wave-vector parameter λ, for three values of the effective wave vector mismatch, $\bar{\beta} = -2, 0, 2$; in each case, the computations were repeated for three different values of the parameter σ. The conclusions of our computations are illustrated in Fig. 7, which shows the dependence on the total beam intensity I_0 of the peak intensity ratios of the two harmonics of the solitons of the averaged system. An important conclusion illustrated by this figure is that, as in the 1D case [42], even small induced cubic nonlinearities can change drastically the characteristics of the QPM solitons. For instance, the peak amplitude ratio at $\sigma = -0.05$ is almost twice as large as its value at $\sigma = 0$. In addition, this change in the soliton characteristics is more pronounced at higher intensities. Thus, the influence of the relative strength of the induced cubic nonlinearities on soliton dynamics increases with the beam intensity. Another phenomenon illustrated in Fig. 7 is that, for positive effective wave vector parameters $\bar{\beta}$, there is a critical threshold of the total beam intensity I_0, below which QPM solitons cannot exist. Furthermore, this threshold intensity depends on the relative strength of the induced cubic nonlinearity σ. This result will be explained in the following section, where soliton stability is studied in detail. Finally, note that for $\sigma \neq 0$ the solitons no longer exist if the total intensity I_0 is larger than some certain threshold. This behavior is not observed in the 1D case.

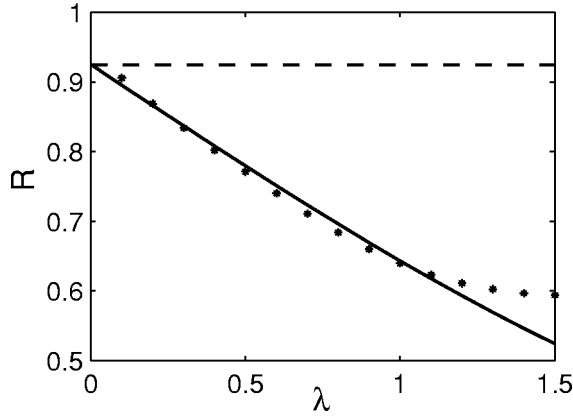In order to investigate the influence of the induced third-

FIG. 8. Peak intensities' ratio $R = |v_0(0,0)|^2 / |u_0(0,0)|^2$ of the soliton solutions of system (10), calculated for $\sigma = 0.05$ (—) and $\sigma = 0$ (- - -), vs soliton parameter λ. The stars correspond to R calculated by numerical integration of system (3). The effective wave-vector mismatch is $\bar{\beta} = 0$.

order nonlinearity on the QPM solitons, we performed the following numerical experiment: we determined the solitons of system (10) that correspond to $\bar{\beta} = 0$ and $\sigma = 0.05$, for several values of the soliton parameter λ. Then, these solutions were used as initial conditions for full system (3) and integrated numerically until a stationary propagation was reached. We then determined the ratio of the peak intensities at the two harmonics and compared the results with those that correspond to the soliton solutions of system (10). The results are presented in Fig. 8. As this figure illustrates, there is a large discrepancy between the predictions of system (10), in which the third-order nonlinearity is taken into account ($\sigma \neq 0$), and the predictions of this system with the third-order nonlinearity neglected ($\sigma = 0$). As one can see, for small soliton wave vectors λ, the former agree well with the numerical simulations of full system (3). Conversely, Fig. 8 shows that for $\lambda \gtrsim 1$ the predictions based on the average model are no longer accurate. The source of this discrepancy can be easily understood by noting that one of the conditions under which the average model was derived is that the average fields must vary slowly with respect to the exponential $e^{i\kappa\zeta}$. This amounts to the requirement that the soliton parameter λ must be much smaller than the grating wave vector κ.

IV. STABILITY ANALYSIS

In this section, we analyze in detail the stability properties of the QPM solitons. In order to do this, we first determine the stability properties of soliton solutions of the averaged system (10) and then we verify whether stable solitons of system (10) remain stable upon propagation in the QPM grating described by full system (3).

It can readily be shown using Eqs. (18) that solitons, or stationary solutions of system (10), correspond to extrema of the functional $H_0 + \lambda I_0$, that is, they satisfy the relation $\delta\{H_0 + \lambda I_0\} = 0$. Here, the soliton wave vector λ plays the role of a Lagrange multiplier. Furthermore, for a fixed I_0, stable solutions correspond to local minima of the Hamil-
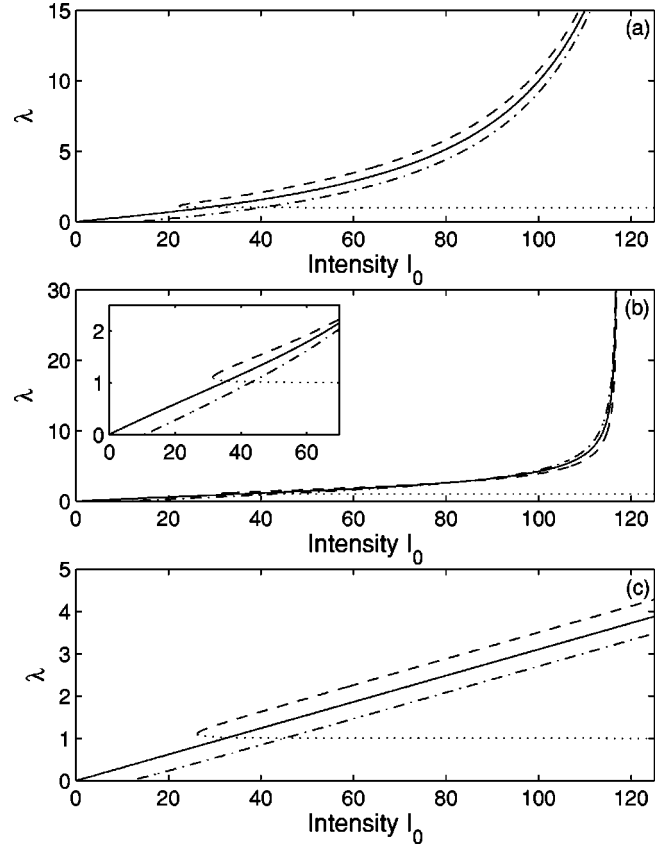

FIG. 9. The intensity I_0 vs soliton wave-vector parameter λ, calculated for $\sigma = -0.05$ (a), $\sigma = 0.05$ (b), and $\sigma = 0$ (c). The effective wave-vector mismatch is $\bar{\beta} = -2$ (- - -), $\bar{\beta} = 0$ (—), and $\bar{\beta} = 2$ ($- \cdot -$); dotted branches correspond to unstable solutions.

tonian H_0, in the function space $\{\tilde{u}_0, \tilde{v}_0\}$, whereas local maxima lead to unstable solutions. Another approach for establishing the stability properties of the soliton solutions uses the Vakhitov-Kolokolov criterion [55], which states that stable solutions correspond to the positive-sloped branches of the function $I_0(\lambda)$. Note that this is only a necessary condition for soliton stability [39]; therefore, we checked by numerical simulations the validity of the results obtained by applying this criterion.

We have determined the functional dependence of the Hamiltonian H_0 and total intensity I_0 on the soliton parameter λ; the dependence of I_0 on λ is presented in Fig. 9. There are several phenomena illustrated by this figure. First, for nonzero effective wave-vector mismatches, $\bar{\beta} \neq 0$, solitons are formed only if the intensity I_0 is above a certain threshold value. Furthermore, for $\bar{\beta} > 0$, the solitons are stable for all values of λ for which they exist, whereas for $\bar{\beta} < 0$ only the solitons that correspond to the upper branch of the multivalued function $\lambda(I_0)$, that is, those that satisfy the Vakhitov-Kolokolov criterion, are stable. For $\bar{\beta} = 0$, stable solitons exist at any intensity I_0. We mention that, for $\bar{\beta} > 0$, the threshold for soliton existence is approximatively given by the relation $I_0^{\text{thr}} = \bar{\beta} I_{\text{NLS}}$, where $I_{\text{NLS}} \simeq 5.85$ is the so-called collapse threshold for the two-dimensional nonlin-
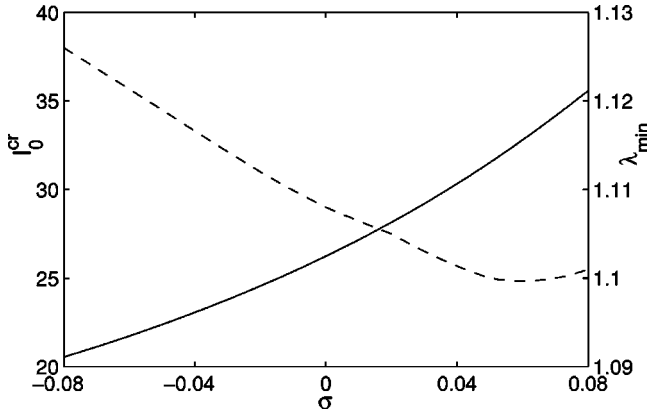
FIG. 10. The critical intensity I_0^{cr} (—) and the corresponding minimum soliton wave vector $\lambda_{\min}$ (- - -) vs induced cubic nonlinearity strength σ.

ear Schrödinger equation model [56–58]. This result has previously been established for 2D solitons in bulk quadratic media [37,41]. The second important fact illustrated in Fig. 9 is that the functional dependence $I_0(\lambda)$ is strongly dependent on the induced cubic nonlinearity strength σ.

To see better the influence of the induced cubic nonlinearity strength σ on the soliton parameters, we present in Fig. 10 the dependence of the critical intensity I_0^{cr} and the corresponding minimum soliton wave vector $\lambda_{\min}$ on the parameter σ. Here, the critical intensity I_0^{cr} is defined as the minimum value of I_0 for which, for $\bar{\beta}<0$, a stable soliton exists. This figure illustrates that variations in σ of only 0.05 produce a change in I_0^{cr} of more than 20%.

In order to verify the results derived from the I_0 vs λ dependency, we determined numerically the dependence of the Hamiltonian H_0 on the total intensity I_0; the results are shown in Fig. 11. Thus, the conclusions suggested by this figure are in complete agreement with those derived from the $I_0(\lambda)$ dependence. For instance, for $\bar{\beta}<0$, the H_0-I_0 diagram has two branches; however, since they correspond to a lower value of the Hamiltonian H_0, only the solitons on the lower branch are stable. This means that, upon propagation, a soliton that corresponds to the upper branch will either decay to radiation or transform into a soliton belonging to the lower branch. This fact can also be derived from the analytic dependence of the Hamiltonian H_0 on the intensity I_0,

$$H_0 = -\frac{1}{2}\lambda I_0 + \frac{1}{4}\bar{\beta}I_{v_0} + \sigma C, \qquad (19)$$

where

$$C = \frac{1}{2}\int\left(\frac{|\tilde{u}_0|^2}{2} - |\tilde{v}_0|^2\right)|\tilde{u}_0|^2 d\eta\, d\xi \qquad (20)$$

is a constant. For $\bar{\beta}<0$, there are two values of the Hamiltonian H_0 that correspond to the same intensity I_0; however, the higher value corresponds to an unstable solution.

To investigate whether these stability properties of the solitons of averaged system (10) can be extended to the
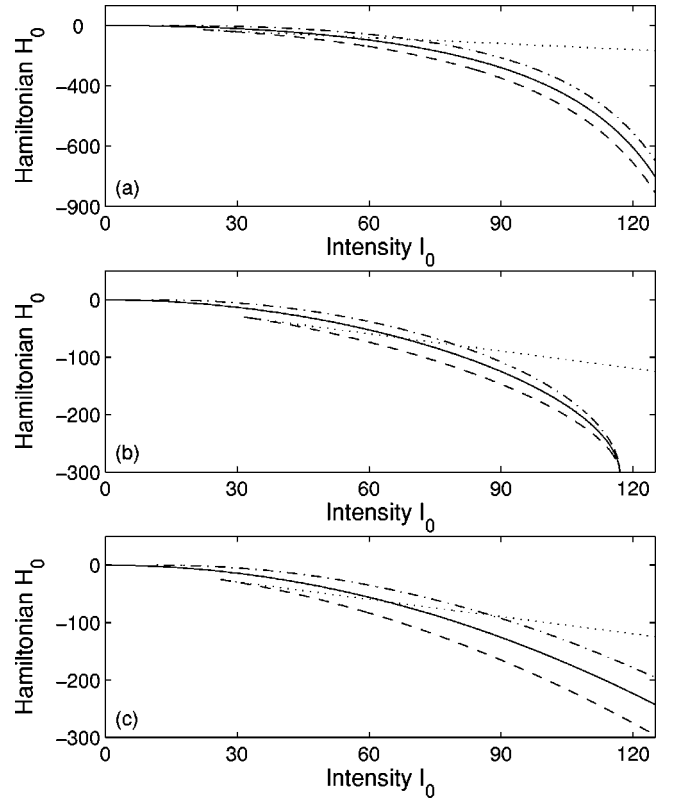

FIG. 11. The Hamiltonian H_0 vs the intensity I_0, calculated for $\sigma=-0.05$ (a), $\sigma=0.05$ (b), and $\sigma=0$ (c). The effective wave-vector mismatch is $\bar{\beta}=-2$ (- - -), $\bar{\beta}=0$ (—), and $\bar{\beta}=2$ ($-\cdot-$); dotted lines correspond to unstable solutions.

QPM solitons of full system (3), we performed an extensive series of numerical simulations. Thus, solitons corresponding to different regions of the H_0-I_0 diagram were converted to the $u-v$ fields by using relations (14), and then the result was used as initial conditions for system (3). With these initial conditions, system (3) was then numerically integrated over a distance $\zeta \sim 35$ diffraction lengths (this limit was imposed by the required computation time). The conclusion of these numerical tests was that stable solitons that correspond to system (10) remain stable upon propagation in the QPM grating described by full system (3).

V. QPM SOLITON EXCITATION FROM GAUSSIAN BEAMS

Since in real experiments one cannot launch into a QPM grating beams with spatial shapes that rigorously match those of specific QPM solitons, it is very important to study whether the QPM solitons described here can be excited from the beams that are more accessible experimentally, that is, Gaussian beams. Therefore, in this section, we examine the characteristics of QPM soliton excitation from Gaussian beams.

We analyze two distinct cases: in the first case, the beams are launched in a SG, whereas in the second case an AG is considered. In both cases, two different experimental conditions are investigated. The first one corresponds to a seeded

SHG experiment, that is, at the input facet of the grating both FW and SH are launched. The second case corresponds to a more common experimental setup, that is, to unseeded SHG, in which case only the FW is launched at the input facet of the grating. In both cases we assume that the gratings are perfectly phase matched, that is, $\bar{\beta} = 0$ ($\beta = \kappa$).

The Gaussian beams launched into the QPM grating are described by the following formulas:

$$u(\eta, \xi; 0) = A_u e^{-r^2/w_u^2}, \tag{21a}$$

$$v(\eta, \xi; 0) = A_v e^{-r^2/w_v^2}, \tag{21b}$$

where $A_{u,v}$ and $w_{u,v}$ are the amplitudes and widths, respectively, of the two Gaussian beams. For these expressions, the relationship between the beam intensity and its parameters is

$$I_{u,v} = \frac{\pi w_{u,v}^2 A_{u,v}^2}{2}. \tag{22}$$

In order to study the soliton excitation from Gaussian beams we proceeded as follows. First, we chose the amplitudes and intensities of the Gaussians at the two harmonics to be equal to those of a QPM soliton that is formed in the specific QPM grating that we analyze. Then, by using Eq. (22), we calculated the corresponding widths of the Gaussians. Before presenting our results, we want to stress an important fact regarding the initial relative phase between the two harmonics. As one can observe from the derivation of the equations describing the QPM solitons, the relative phase between the two harmonics that form a QPM soliton is equal to $\pi/2$. It has been established [59] that this value of the initial relative phase between the two harmonics corresponds to a case in which, during the process of soliton formation, it emits the smallest amount of radiation. Therefore, in what follows, we choose one of the amplitudes to be real, while the other one is purely imaginary.

We started by launching the Gaussian beams in the SG described in Sec. III and the results are presented in Fig. 12. Figure 12(a) shows the results corresponding to the seeded SHG. The beams' parameters were calculated by following the procedure previously described. However, in order to compensate for the larger amount of radiation emitted, as compared to the case when into the grating are launched exact QPM solitons, the intensities of the two beams were slightly larger than those corresponding to the soliton in Fig. 2. Figure 12(a) shows that, as compared to the case of soliton propagation, which was described in Sec. III, the transient distance over which the solitons are formed is slightly longer; however, the intensities of the solitons that eventually form are very close to those that correspond to the case when pure solitons are launched into the QPM grating. In the unseeded SHG case, presented in Fig. 12(b), the transient distance over which the beams reshape to form a stable QPM soliton is much longer. In addition, the amount of radiation shed off by the beams is larger, a consequence of the fact that the input beams are very different from a pure soliton solution. However, after the beams propagate a certain distance, in this case too a QPM soliton is formed.
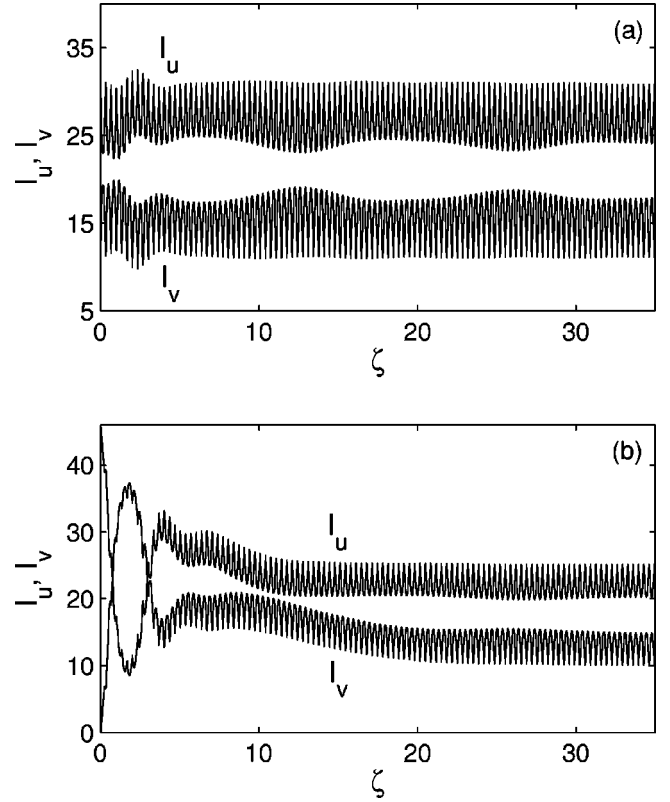

FIG. 12. Evolution of the intensities of Gaussian beams launched in a SG characterized by the following parameters: $a_u = a_v = 0$, $\gamma_0 = 0$, $\gamma = 1$, and $\kappa = 9.35$. The parameters of the input beams are (a) $A_u = 2.92$, $A_v = 1.8$, $w_u = 1.52$, and $w_v = 1.49$ (seeded SHG); (b) $A_u = 3$, $A_v = 10^{-2}$, $w_u = 1.8$, and $w_v = 1$ (unseeded SHG).

In Fig. 13 we show the results of the propagation of the Gaussian beams in the AG described in Sec. III. This figure shows that in the case of the AG, when compared to the SG case, the dynamics of the interacting beams during the transient regime is more complex. Moreover, the amount of radiation emitted during the process of soliton formation is larger in this case, too. This result can be explained by the fact that the adjacent domains in an AG have different refractive indices, so that the beams are scattered at the domain interfaces. However, in the case of AG too, after a certain transient regime, QPM solitons are formed in both seeded and unseeded numerical experiments.

To conclude this section, we mention that we repeated the numerical experiments described above, for different values of the QPM grating and beam parameters. The conclusion was that although we obtained different quantitative results, the general characteristics of the process of soliton excitation from the Gaussian beams were similar to those described above.

VI. CONCLUSIONS

In conclusion, we have studied both the formation of two-dimensional solitons in a QPM grating as well as their stability properties upon propagation. The QPM gratings taken into account covered two distinct classes: in the first case,
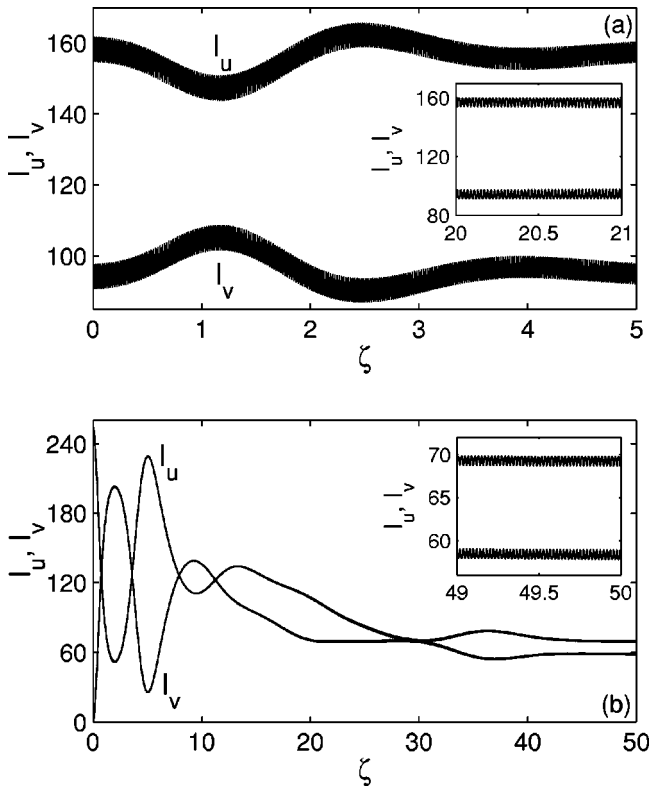
FIG. 13. Evolution of the intensities of Gaussian beams launched in an AG characterized by the following parameters: $a_u = 1$, $a_v = 1.928$, $\gamma_0 = 1$, $\gamma = 0.4$, and $\kappa = 308.42$. The parameters of the input beams are (a) $A_u = 6.28$, $A_v = 5.49$, $w_u = 1.52$, and $w_v = 1.49$ (seeded SHG); (b) $A_u = 7.07$, $A_v = 10^{-2}$, $w_u = 1.8$, and $w_v = 1$ (unseeded SHG). In the insets, beam profiles calculated after the stationary propagation are reached (one diffraction length is shown).

SG were considered, that is, only the quadratic nonlinearity coefficient was periodically modulated, whereas in the second case, AG gratings, both the quadratic nonlinear coefficient and the refractive indices at the two harmonics were periodic functions with respect to the longitudinal distance. It has been demonstrated that in both cases, in the first order of an asymptotic perturbation theory, the beam dynamics is strongly influenced by an induced third-order Kerr-like nonlinearity. A detailed description of the influence of this induced cubic nonlinearity on the QPM soliton dynamics and their stability properties has been presented. Thus, it has been shown that this cubic nonlinearity can shift by more that 20% the threshold intensity above which the solitons can exist, both for positive and negative effective phase mismatches. The conclusions derived from the first-order

asymptotic analysis were verified by numerical integration of the complete set of equations that describes beam propagation in a QPM grating.

We also discussed the excitation of QPM solitons by Gaussian beams. For both types of the QPM gratings considered here, SG and AG, we demonstrated that QPM solitons can be obtained from Gaussian beams, when either both harmonics are injected into the grating (seeded SHG) or only the FW is inserted into the grating (unseeded SHG). We demonstrated that when SG are used, the amount of energy that is radiated over the transient distance over which the soliton is formed is smaller as compared to that that corresponds to the case of soliton generation in AG. We also showed that, in both cases, after a transient regime during which part of the input energy is radiated out, stable QPM solitons are formed.

As an important remark, we mention that the QPM solitons investigated in this paper are very similar to the guiding-center solitons that can propagate in an optical fiber link that contains optical amplifiers, periodically inserted in the transmission line [60]. As in the case of QPM solitons discussed here, guiding-center solitons in optical fibers are formed when the characteristic length associated to the periodicity of the system (the distance between amplifiers) is much smaller than the characteristic length associated to the dynamics of the pulses (the dispersion length). However, the averaged nonlinear equation describing the guiding-center solitons in optical fibers does not contain nonlinearities of higher order, as compared to the original equation, the nonlinear Schrödinger equation. Based on this similarity, one expects to observe a set of new and interesting phenomena when the grating period becomes commensurable with the soliton diffraction length. For instance, in such a case, it is expected to observe a resonant radiative reshaping of the QPM solitons whose parameters satisfy this condition.

Finally, we mention that the results presented here could be applied to other optical structures containing periodically alternating slabs of materials with different optical properties, e.g., Kerr-layered structures [61,62], or tandem structures where the nonlinearity and the group velocity dispersion are spatially distributed between the adjacent slabs [63].

ACKNOWLEDGMENTS

[1] J.A. Armstrong, N. Bloembergen, J. Ducuing, and P.S. Pershan, Phys. Rev. **127**, 1918 (1962).

[2] N.R. Belashenkov, S.V. Gagarsky, and M.V. Inochkin, Opt. Spectrosk. **66**, 1383 (1989) [Opt. Spectrosc. **66**, 806 (1989)].

[3] G.I. Stegeman, M. Sheik-Bahae, E.W. Van Stryland, and G.

Assanto, Opt. Lett. **18**, 13 (1993).

[4] A. Kobyakov and F. Lederer, Phys. Rev. A **54**, 3455 (1996).

[5] R. DeSalvo, D.J. Hagan, M. Sheik-Bahae, G.I. Stegeman, E.W. Van Stryland, and H. Vanherzeele, Opt. Lett. **17**, 28 (1992).

[6] R. Schiek, J. Opt. Soc. Am. B **10**, 1848 (1993); J. Opt. Quan-

tum Electron. **26**, 415 (1994).

[7] M.L. Sundheimer, C. Bosshard, E.W. Van Stryland, G.I. Stegeman, and J.D. Bierlein, Opt. Lett. **18**, 1397 (1993); M.L. Sundheimer, A. Villeneuve, G.I. Stegeman, and J.D. Bierlein, Electron. Lett. **30**, 1400 (1994).

[8] D.C. Hutchings, S. Aitchison, and C.N. Ironside, Opt. Lett. **18**, 793 (1993).

[9] Y. Baek, R. Schiek, and G.I. Stegeman, Opt. Lett. **20**, 2168 (1995).

[10] R. Schiek, Y. Baek, G. Krijnen, G.I. Stegeman, I. Bauman, and W. Sohler, Opt. Lett. **21**, 940 (1996).

[11] R. Schiek, M.L. Sundheimer, D.Y. Kim, Y. Baek, G.I. Stegeman, H. Seibert, and W. Sohler, Opt. Lett. **19**, 1949 (1994).

[12] D.J. Hagan, Z. Wang, G.I. Stegeman, E.W. Van Stryland, M. Sheik-Bahae, and G. Assanto, Opt. Lett. **19**, 1305 (1994).

[13] U. Trutschel, U. Langbein, F. Lederer, and H.E. Ponath, IEEE J. Quantum Electron. **21**, 1639 (1985).

[14] C.N. Ironside, S. Aitchison, and J.M. Arnold, IEEE J. Quantum Electron. **29**, 2650 (1993).

[15] G. Assanto, G.I. Stegeman, M. Sheik-Bahae, and E.W. Van Stryland, Appl. Phys. Lett. **62**, 1323 (1993).

[16] P.St.J. Russel, Electron. Lett. **29**, 1228 (1993).

[17] G. Assanto, I. Torelli, and S. Trillo, Opt. Lett. **19**, 1720 (1994).

[18] G. Assanto, Z. Wang, D.J. Hagan, and E.W. Van Stryland, Appl. Phys. Lett. **67**, 2120 (1995).

[19] L. Lefort and A. Barthelemy, Electron. Lett. **31**, 910 (1995).

[20] A. Kobyakov, U. Peschel, R. Muschall, G. Assanto, V.P. Torchigin, and F. Lederer, Opt. Lett. **20**, 1686 (1995).

[21] L. Lefort and A. Barthelemy, Opt. Commun. **119**, 163 (1995).

[22] Y.R. Shen, *The Principles of Nonlinear Optics* (Wiley, New York, 1984).

[23] A. Yariv, *Optical Electronics in Modern Communications* (Oxford University Press, New York, 1996).

[24] M.M. Fejer, G.A. Magel, D.H. Jundt, and R.L. Byer, IEEE J. Quantum Electron. **28**, 2631 (1992); K. Yamamoto, K. Mizuuchi, and T. Taniuchi, *ibid.* **28**, 1909 (1992).

[25] J. Webjorn, V. Pruneri, P.St.J. Russel, J.R.M. Barr, and D.C. Hanna, Electron. Lett. **30**, 894 (1994).

[26] Q. Chen and W.P. Risk, Electron. Lett. **30**, 1516 (1994).

[27] E.J. Lim, H.M. Herka, M.L. Bortz, and M.M. Fejer, Appl. Phys. Lett. **59**, 2207 (1991).

[28] D. Hofmann, G. Schreiber, C. Haase, H. Herrmann, R. Ricken, and W. Sohler, Opt. Lett. **24**, 896 (1999).

[29] A.M. Radojevic, M. Levy, R.M. Osgood, D.H. Jundt, A. Kumar, and H. Bakhru, Opt. Lett. **25**, 1034 (2000).

[30] A.S. Helmy, D.C. Hutchings, T.C. Kleckner, J.H. Marsh, A.C. Bryce, J.M. Arnold, C.R. Stanley, J.S. Aitchison, C.T.A. Brown, K. Moutzouris, and M. Ebrahimzadeh, Opt. Lett. **25**, 1370 (2000).

[31] S.J. Yoo, R. Bhat, C. Caneau, and M.A. Koza, Appl. Phys. Lett. **66**, 3410 (1995).

[32] A. Fiore, S. Janz, L. Delobel, P. van der Meer, P. Bravetti, V. Berger, and E. Rosencher, Appl. Phys. Lett. **72**, 2942 (1998).

[33] Y. Shuto, T. Watanabe, S. Tomaru, I. Yokohama, M. Hikita, and M. Amano, IEEE J. Quantum Electron. **33**, 349 (1997).

[34] W.E. Torruellas, Z. Wang, D.J. Hagan, E.W. Van Stryland, G.I. Stegeman, L. Torner, and C.R. Menyuk, Phys. Rev. Lett. **74**, 5036 (1995).

[35] R. Schiek, Y. Baek, and G.I. Stegeman, Phys. Rev. E **53**, 1138 (1996).

[36] A.V. Buryak and Y.S. Kivshar, Opt. Lett. **19**, 1612 (1994); L. Torner, C.R. Menyuk, and G.I. Stegeman, *ibid.* **19**, 1615 (1994); D.E. Pelinovsky, A.V. Buryak, and Y.S. Kivshar, Phys. Rev. Lett. **75**, 591 (1995); L. Torner, D. Mihalache, D. Mazilu, and N.N. Akhmediev, Opt. Lett. **20**, 2183 (1995).

[37] L. Torner, D. Mihalache, D. Mazilu, E.M. Wright, W.E. Torruellas, and G.I. Stegeman, Opt. Commun. **121**, 149 (1995).

[38] L. Berge, V.K. Mezentsev, J.J. Rasmussen, and J. Wyller, Phys. Rev. A **52**, R28 (1995); L. Berge, O. Bang, J.J. Rasmussen, and V.K. Mezentsev, Phys. Rev. E **55**, 3555 (1997).

[39] O. Bang, Y.S. Kivshar, A.V. Buryak, A. De Rossi, and S. Trillo, Phys. Rev. E **58**, 5057 (1998).

[40] L. Torner, D. Mazilu, and D. Mihalache, Phys. Rev. Lett. **77**, 2455 (1996).

[41] D. Mihalache, D. Mazilu, L.C. Crasovan, and L. Torner, Opt. Commun. **137**, 113 (1997).

[42] C.B. Clausen, O. Bang, and Y.S. Kivshar, Phys. Rev. Lett. **78**, 4749 (1997); J.F. Corney and O. Bang, *ibid.* **87**, 133901 (2001); Phys. Rev. E **64**, 047601 (2001).

[43] C.B. Clausen, Y.S. Kivshar, O. Bang, and P.L. Christiansen, Phys. Rev. Lett. **83**, 4740 (1999).

[44] O. Bang and J.F. Corney, Opt. Photonics News **12**, 42 (2001); J.F. Corney and O. Bang, J. Opt. Soc. Am. B **19**, 812 (2002).

[45] O. Bang, C.B. Clausen, P.L. Christiansen, and L. Torner, Opt. Lett. **24**, 1413 (1999).

[46] A. Kobyakov, F. Lederer, O. Bang, and Y.S. Kivshar, Opt. Lett. **23**, 506 (1998); O. Bang, T.W. Graversen, and J.F. Corney, *ibid.* **26**, 1007 (2001).

[47] B. Bourliaguet, V. Couderc, A. Barthelemy, G.W. Ross, P.G.R. Smith, D.C. Hanna, and C. De Angelis, Opt. Lett. **24**, 1410 (1999).

[48] C. Etrich, F. Lederer, B.A. Malomed, T. Peschel, and U. Peschel, in *Progress in Optics*, edited by E. Wolf (North Holland, Amsterdam, 2000), Vol. 41, pp. 483–568; A.V. Buryak, P. Di Trapani, D.V. Skryabin, and S. Trillo, Phys. Rep. **370**, 63 (2002).

[49] C.R. Menyuk, R. Schiek, and L. Torner, J. Opt. Soc. Am. B **11**, 2434 (1994).

[50] S.K. Johansen, S. Carrasco, L. Torner, and O. Bang, Opt. Commun. **203**, 393 (2002).

[51] P. Di Trapani, A. Bramati, S. Minardi, W. Chinaglia, C. Conti, S. Trillo, J. Kilius, and G. Valiulis, Phys. Rev. Lett. **87**, 183902 (2001).

[52] D. Mihalache, L.C. Crasovan, and N.C. Panoiu, J. Phys. A **30**, 5855 (1997).

[53] J.M. Ortega and W.C. Rheinboldt, *Iterative Solution of Nonlinear Equations in Several Variables* (Academic Press, New York, 1970), p. 182.

[54] G. Dahlquist and A. Bjork, *Numerical Methods* (Prentice Hall, Englewood Cliffs, NJ, 1974).

[55] M.G. Vakhitov and A.A. Kolokolov, Radiophys. Quantum Electron. **16**, 783 (1973).

[56] M.I. Weinstein, Commun. Math. Phys. **87**, 567 (1983).

[57] Y. Silberberg, Opt. Lett. **15**, 1282 (1990).

[58] D. Mihalache, D. Mazilu, B.A. Malomed, and L. Torner, Opt. Commun. **152**, 365 (1998).

[59] L. Torner and G.I. Stegeman, J. Opt. Soc. Am. B **14**, 3127 (1997).

[60] A. Hasegawa and Y. Kodama, Phys. Rev. Lett. **66**, 161 (1991); Y. Kodama and A. Hasegawa, Prog. Opt. **30**, 205 (1992).

[61] L. Berge, V.K. Mezentsev, J.J. Rasmussen, P.L. Christiansen,

and Yu.B. Gaididei, Opt. Lett. **25**, 1037 (2000).

[62] I. Towers and B.A. Malomed, J. Opt. Soc. Am. B **19**, 537 (2002).

[63] L. Torner, S. Carrasco, J.P. Torres, L.C. Crasovan, and D. Mihalache, Opt. Commun. **199**, 277 (2001).